Anomalous spatial shifts in interface electronic reflection beyond the linear approximation

Runze Li,[1,2] Chaoxi Cui,[1,2,*] Xinxing Zhou,[3,†] and Zhi-Ming Yu[1,2]

[1]*Centre for Quantum Physics, Key Laboratory of Advanced Optoelectronic Quantum Architecture and Measurement (MOE), School of Physics, Beijing Institute of Technology, Beijing 100081, China*

[2]*Beijing Key Lab of Nanophotonics & Ultrafine Optoelectronic Systems, School of Physics, Beijing Institute of Technology, Beijing 100081, China*

[3]*Key Laboratory of Low-Dimensional Quantum Structures and Quantum Control of Ministry of Education, Synergetic Innovation Center for Quantum Effects and Applications, School of Physics and Electronics, Hunan Normal University, Changsha 410081, China*

(Received 12 December 2022; accepted 1 August 2023; published 21 August 2023)

Recently, the electronic analogy of the anomalous spatial shift, including Goos-Hänchen and Imbert-Fedorov effects, has been attracting widespread interest. Current research on the anomalous spatial shift in interface electronic reflection is based on the paradigm of linear approximation, under which the center position of the incident and reflected beams are obtained by expanding the phases of relevant basis states and scattering amplitudes to the first order of incident momentum. However, in a class of normal cases, the linear approximation leads to divergent spatial shifts in reflection for certain incident angles, even though the corresponding reflection possibility is finite. In this paper, we show that these nonphysical results are caused by an abrupt change in the number of the propagating states at critical parameters, and can be resolved by calculating the center positions of the scattering beams beyond the linear approximation. Moreover, we find that the beam width has an important influence on the spatial shift near the critical angles. We demonstrate our idea via concrete calculations of Goos-Hänchen and Imbert-Fedorov shift on two representative models. These results provide a deeper understanding of the anomalous spatial shift in calculations.

DOI: 10.1103/PhysRevB.108.075149

I. INTRODUCTION

According to the laws of reflection in geometric optics, one knows that the incident point is always the same as the point where the light beam is reflected back at a sharp interface. However, due to the wave nature of photons, these laws should be revised in certain cases and a light beam can experience an anomalous spatial shift under reflection, namely, there exists a shift between the incident and the reflected beams at the interface [1]. Generally, the spatial shift is divided into longitudinal and transverse components with respect to the incident plane, known as the Goos-Hänchen shift [2,3] and Imbert-Fedorov shift [4–6], respectively. Since the wave-particle duality is a foundational concept in physics and holds for all particles, the anomalous spatial shift can also be found in many other particles, such as electrons [7–13], atoms [14], and neutrons [15].

In electronic systems, the valence and conduction bands can cross around the Fermi level, leading to nontrivial band degeneracy [16–24]. The band degeneracies in three-dimensional (3D) topological semimetals have many different types, and can be classified as a 0D nodal point, 1D nodal line, and 2D nodal surface [25–27]. Remarkably, in the interface constructed by topological semimetals and other systems, both longitudinal and transverse shift effects are generally significant, due to strong (pseudo)spin-orbit coupling in topological semimetals [8,28–31]. Such a significant anomalous spatial shift can lead to various physical consequences, such as chirality-dependent Hall effect [29] and modifying the dispersion of the confined waveguide modes [8]. Moreover, the behavior of the longitudinal and transverse shifts in these systems has a strong dependence on the species of the band degeneracies [28–31]. For example, when a beam comes from normal metal onto the interface with topological Weyl semimetals, there will exist quantum vortices in the vector field of the spatial shift in the interface momentum space, and the number of quantum vortices is determined by the topological charge of the Weyl points [32]. The anomalous shifts can also be realized in Andreev reflection, during which the incident particle changes its identity from electron to hole [33–36]. Similarly, the shifts strongly depend on the pair potential of the superconductors, which in turn can be used to probe the superconducting states.

Currently, the standard and the most general approach used to study the anomalous shifts in electronic systems is the quantum scattering approach under linear approximation [11]. In this approach, the incident beam is modeled by wave packet Ψ, which is constructed by the incident basis states $\psi^i(\boldsymbol{k})$ and is confined in both real and momentum spaces $(\boldsymbol{r}^c, \boldsymbol{k}^c)$. During scattering, the wave packet would be reconstructed, as each incident basis state $\psi^i(\boldsymbol{k})$ is scattered into reflected basis state $\psi^r(\boldsymbol{k})$ with a certain reflection amplitude. The anomalous

*cuichaoxi@bit.edu.cn
†xinxingzhou@hunnu.edu.cn

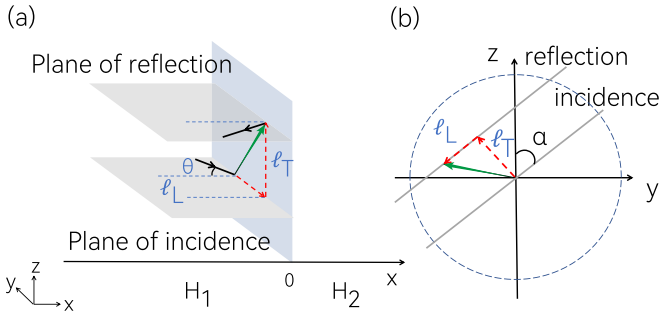

FIG. 1. (a) Schematic figure showing the anomalous spatial shift $\boldsymbol{\ell}$ in interface scattering. (b) Top view of the $y-z$ plane in (a).

shifts then are obtained by comparing the center position of the incident and reflected beams. In practice, one generally chooses the wave-packet profile to have a Gaussian form and, in such case, the anomalous shifts can be analytically obtained by expanding the phases of the relevant scattering basis states $[\psi^i(\boldsymbol{k})$ and $\psi^r(\boldsymbol{k})]$ and reflection amplitudes to the linear order around $\boldsymbol{k}^c$.

The linear approximation is valid for most cases and gives accurate analytical results, which are helpful for gaining insight into the physics of the shifts. However, for a class of normal cases, the linear approximation leads to a divergence of the anomalous shifts in reflection at certain incident angles, even when the corresponding reflection possibility is finite [8,28,35]. In previous work, Liu *et al.* demonstrated that the spectral singularities in parity-time symmetric systems, which arise due to the assumption of linearity of the medium, can be removed by considering all-order nonlinearity [37]. Then two important questions arise: Under what conditions does the linear approximation not apply? And is it possible to resolve the divergences by taking all-order nonlinearity into account or by establishing an alternative approximation?

In this paper, we show that the divergence of the shifts in linear approximation are closely related to an abrupt change of the number of propagating states. In scattering, while the number of the scattering states is fixed, the number of the propagating states is not, and may abruptly change when some critical parameters like incident angle or Fermi energy change. This abrupt change would lead to a singularity in reflection amplitude or its derivative, which in the framework of linear approximation inevitably results in divergent anomalous shifts. We show this divergence can be resolved by calculating the center position of the incident and reflected beams beyond the linear approximation. We explicitly demonstrate our idea by calculating the longitudinal (Goos-Hänchen) and transverse (Imbert-Fedorov) shifts on two representative models and by two different methods. Our paper will be beneficial for clarifying the scope of application of the linear approximation in the study of anomalous spatial shifts.

II. QUANTUM SCATTERING APPROACH

Consider a general model which contains two media, respectively, described by Hamiltonians H_1 and H_2, and a flat interface between these two media, as illustrated in Fig. 1(a). We also assume that the junction model is extended along y and z directions, indicating that k_y and k_z are conserved quantities during scattering. A beam of particles is incoming from the region of $x<0$ (H_1) and is scattered at the interface residing at the $x=0$ plane. Besides, there is a rotation angle α between the incident plane and the y axis, as shown in Fig. 1(b).

To define the anomalous spatial shift, the incident beam should be modeled by a wave packet, which is required to be confined in both real and momentum spaces. We choose the wave-packet profile to have a Gaussian form. Then, an incident wave packet centered at $\boldsymbol{k}^c=(k_y^c,k_z^c)$ can be written as [8,11]

$$\Psi^i(\boldsymbol{r},\boldsymbol{k}^c)=\int w(\boldsymbol{k}-\boldsymbol{k}^c)\psi^i(\boldsymbol{k})d\boldsymbol{k}, \tag{1}$$

where $\psi^i(\boldsymbol{k})=e^{i\boldsymbol{k}\cdot\boldsymbol{r}}|u^i(\boldsymbol{k})\rangle$ is the Bloch eigenstate of the incident medium and $|u^i(\boldsymbol{k})\rangle$ is the cell-periodic part of the eigenstate. The wave-packet profile w reads

$$w(\boldsymbol{k})=\prod_{i=y,z}(\sqrt{2\pi}W_i)^{-1}e^{-k_i^2/(2W_i^2)}, \tag{2}$$

where W_i denotes the Gaussian width for the ith component, controlling the beam width in momentum space. The center position of the incident beam can be written as [38,39]

$$\boldsymbol{r}_i^c(\boldsymbol{k}^c)=\frac{\int\boldsymbol{r}|\Psi^i(\boldsymbol{r},\boldsymbol{k}^c)|^2d\boldsymbol{r}}{\int|\Psi^i(\boldsymbol{r},\boldsymbol{k}^c)|^2d\boldsymbol{r}}. \tag{3}$$

When the incident beam hits the interface, each partial wave $\psi^i(\boldsymbol{k})$ is scattered into the reflected basis state $\psi^r(\boldsymbol{k})$ with a certain $\boldsymbol{k}$-dependent reflection amplitude $A_r(\boldsymbol{k})$. The reflection amplitude here is obtained by the standard quantum scattering approach. Then, the reflected beam also is a wave packet and can be expressed as

$$\Psi^r(\boldsymbol{r},\boldsymbol{k}^c)=\int w(\boldsymbol{k}-\boldsymbol{k}^c)A_r(\boldsymbol{k})\psi^r(\boldsymbol{k})d\boldsymbol{k}, \tag{4}$$

and its center position is

$$\boldsymbol{r}_r^c(\boldsymbol{k}^c)=\frac{\int\boldsymbol{r}|\Psi^r(\boldsymbol{r},\boldsymbol{k}^c)|^2d\boldsymbol{r}}{\int|\Psi^r(\boldsymbol{r},\boldsymbol{k}^c)|^2d\boldsymbol{r}}. \tag{5}$$

By comparing the center position of the incident and reflected beam, the anomalous shift in reflection is obtained as

$$\boldsymbol{\ell}(\boldsymbol{k}^c)=\boldsymbol{r}_r^c(\boldsymbol{k}^c)-\boldsymbol{r}_i^c(\boldsymbol{k}^c), \tag{6}$$

which is a vector and forms a vector field in the interface momentum space. However, it should be noted that based on Eq. (6), while one always can numerically obtain $\boldsymbol{\ell}(\boldsymbol{k}^c)$, it is impossible to obtain an analytical expression for $\boldsymbol{\ell}(\boldsymbol{k}^c)$, which prevents a deep understanding of the physics underlying the shifts. To resolve this problem, one has to resort to linear approximation, as it can give an analytical expression of $\boldsymbol{\ell}(\boldsymbol{k}^c)$ in many cases.

The Bloch eigenstate of the incident medium may include multiple (N) components, i.e., $|u^{i(r)}(\boldsymbol{k})\rangle=(u_1^{i(r)},\cdots u_N^{i(r)})^T$, then the wave packets $\Psi^{i(r)}$ should also have N components. The nth component of Ψ^i and Ψ^r are, respectively, expressed as

$$\Psi_n^i(\boldsymbol{r},\boldsymbol{k}^c)=\int d\boldsymbol{k}w(\boldsymbol{k}-\boldsymbol{k}^c)e^{i\boldsymbol{k}\cdot\boldsymbol{r}}\left|u_n^i(\boldsymbol{k})\right|e^{i\phi_n^i(\boldsymbol{k})} \tag{7}$$

and

$$\Psi_n^r(\boldsymbol{r},\boldsymbol{k}^c)=\int d\boldsymbol{k}\,w(\boldsymbol{k}-\boldsymbol{k}^c)|A_r|e^{i\varphi(\boldsymbol{k})}e^{i\boldsymbol{k}\cdot\boldsymbol{r}}\left|u_n^r(\boldsymbol{k})\right|e^{i\phi_n^r(\boldsymbol{k})}, \quad (8)$$

with $\phi_n^{i(r)}(\boldsymbol{k})=\arg[u_n^{i(r)}(\boldsymbol{k})]$ and $\varphi(\boldsymbol{k})=\arg[A_r(\boldsymbol{k})]$. In the framework of linear approximation, the two phases $\phi_n^{i(r)}(\boldsymbol{k})$ and $\varphi(\boldsymbol{k})$ in Eqs. (7) and (8) are replaced by the first-order Taylor series expanded around $\boldsymbol{k}^c$:

$$\phi_n^{i(r)}(\boldsymbol{k})=\phi_n^{i(r)}(\boldsymbol{k}^c)+(\boldsymbol{k}-\boldsymbol{k}^c)\cdot\partial_{\boldsymbol{k}}\phi_n^{i(r)}\big|_{\boldsymbol{k}=\boldsymbol{k}^c}, \quad (9)$$

$$\varphi(\boldsymbol{k})=\varphi(\boldsymbol{k}^c)+(\boldsymbol{k}-\boldsymbol{k}^c)\cdot\partial_{\boldsymbol{k}}\varphi|_{\boldsymbol{k}=\boldsymbol{k}^c}. \quad (10)$$

With the linear approximation, one can find that Eqs. (7) and (8) will take the following forms:

$$\Psi_n^i(\boldsymbol{r},\boldsymbol{k}^c)\propto e^{-W_y^2(y+\partial_{k_y}\phi_n^i|_{\boldsymbol{k}=\boldsymbol{k}^c})^2/2}e^{-W_z^2(z+\partial_{k_z}\phi_n^i|_{\boldsymbol{k}=\boldsymbol{k}^c})^2/2}, \quad (11)$$

$$\Psi_n^r(\boldsymbol{r},\boldsymbol{k}^c)\propto e^{-W_y^2(y+\partial_{k_y}(\phi_n^r+\varphi)|_{\boldsymbol{k}=\boldsymbol{k}^c})^2/2}e^{-W_z^2(z+\partial_{k_z}(\phi_n^r+\varphi)|_{\boldsymbol{k}=\boldsymbol{k}^c})^2/2}, \quad (12)$$

indicating that Ψ_n^i and Ψ_n^r are centered at $-\partial_{\boldsymbol{k}}\phi_n^i|_{\boldsymbol{k}=\boldsymbol{k}^c}$ and $-\partial_{\boldsymbol{k}}(\phi_n^r+\varphi)|_{\boldsymbol{k}=\boldsymbol{k}^c}$, respectively. The center position of incident and reflected beams are the average of all components, written as

$$\boldsymbol{r}_i^c=-\sum_n v_n^i\partial_{\boldsymbol{k}}\phi_n^i\big|_{\boldsymbol{k}=\boldsymbol{k}^c}, \quad (13)$$

$$\boldsymbol{r}_r^c=-\sum_n v_n^r\partial_{\boldsymbol{k}}\left(\phi_n^r+\varphi\right)\big|_{\boldsymbol{k}=\boldsymbol{k}^c}, \quad (14)$$

with $v_n^{i(r)}$ the weight of the nth component of $|u^{i(r)}\rangle$, satisfying $\sum_n(v_n^{i(r)})^2=1$. Hence, the anomalous shift from linear approximation can be analytically expressed as the difference between the two center positions:

$$\boldsymbol{\ell}^{\mathrm{LA}}=\sum_n\left[v_n^i\partial_{\boldsymbol{k}}\phi_n^i\big|_{\boldsymbol{k}=\boldsymbol{k}^c}-v_n^r\partial_{\boldsymbol{k}}\left(\phi_n^r+\varphi\right)\big|_{\boldsymbol{k}=\boldsymbol{k}^c}\right]. \quad (15)$$

This expression is equivalent to the shift vector obtained in Ref. [40]. By analyzing the above derivation, we find that there are two prerequisites for application of the linear approximation: (1) After scattering, the reflected beams should still be centered at $\boldsymbol{k}^c$ in momentum space. (2) The reflection amplitude $A_r(\boldsymbol{k})$ should be an analytic function in the neighborhood of $\boldsymbol{k}^c$, as it is a prerequisite for the Taylor expansion of $\arg[A_r(\boldsymbol{k})]$.

These two conditions can be satisfied for most cases. Generally, condition Eq. (1) is always satisfied except if the reflection probability is vanishing at $\boldsymbol{k}=\boldsymbol{k}^c$. But, in such case, the anomalous shift would be irrelevant for physical observations, as no particle is reflected back and then the anomalous shift will not happen. In contrast, we show that the condition Eq. (2) does not hold at certain incident angles and model parameters, beyond which the number of the scattered propagating states changes. This abrupt change generally leads to divergent shifts [obtained from linear approximation Eq. (15)] at the critical parameters, which apparently are not correct. Hence, to obtain correct results, we have to calculate the anomalous shifts via Eq. (6). We find that at the critical parameters, the anomalous shifts obtained from Eq. (6) are completely different from that obtained from linear approximation Eq. (15), and are not divergent. Away from the critical parameters, the anomalous shifts obtained from both approaches are almost the same. In addition, the anomalous shifts around (away from) the critical parameters have a strong (negligible) dependence on the beam width W. In the following, we use two representative examples to demonstrate our ideas.

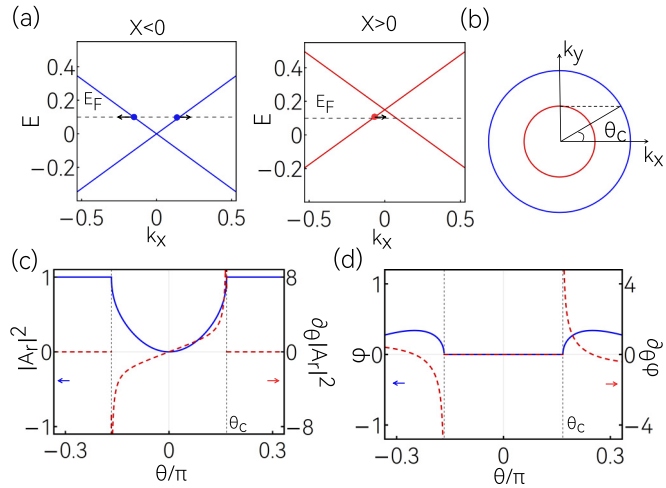

FIG. 2. (a) The band structure of incident medium ($x<0$) and transmitted medium ($x>0$) in model Eq. (16). The spheres denote the incident, reflected, and transmitted electron states, and the arrows indicate their moving directions. (b) The Fermi surfaces of both $x<0$ (blue circle) and $x>0$ (red circle) mediums with the label of the critical angel θ_c. (c) $|A_r|^2$ and its derivative and (d) the phase $\varphi=\arg(A_r)$ and its derivative versus incident angle θ. In the calculation, we choose $E_F=100$ meV, $V=150$ meV, and $v=10^6$ m/s.

III. LONGITUDINAL SHIFT IN GRAPHENE MODEL

In the first case, we consider a graphene junction model. This model is simple and features a divergent longitudinal spatial shift with finite reflection probability, as demonstrated in Ref. [8]. Similar divergence in longitudinal spatial shift also can be found in the Weyl semimetals [28,29]. However, the origin of the divergence has not been discussed there. Here, we will show the divergence is caused by an abrupt change of scattering environment.

According to the setup in Fig. 1, we assume the junction model is lied on the $x-y$ plane. Notice that the z direction here is a dummy degree of freedom, as graphene is a 2D system and the longitudinal shift is within the scattering plane. The Hamiltonian of the junction model is given as [8]

$$\mathcal{H}=\begin{cases}vk_x\sigma_x+vk_y\sigma_y, & x<0\\ vk_x\sigma_x+vk_y\sigma_y+V, & x>0,\end{cases} \quad (16)$$

where v is the fermi velocity, σ is the Pauli matrix, and V denotes a potential energy applied on the $x>0$ region.

We plot the band structure of the graphene model in both $x<0$ and $x>0$ regions in Fig. 2(a) and the corresponding equienergy contours in Fig. 2(b). The possible incident and reflected electron states are also marked in Fig. 2(a). One can find that for a fixed Fermi energy $E_F>0$ (measured from the Dirac point) and a finite V satisfying $0<V<2E_F$, there exists two critical incident angles $\pm\theta_c$, beyond which there is

no propagating mode for the transmitted state [see Fig. 2(b)]. The critical angle is given as

$$\theta_c = \arcsin\left|\frac{V - E_F}{E_F}\right|. \tag{17}$$

When the incident angle $\theta = \arctan(k_y/k_x)$ is smaller than the critical angle $|\theta| < \theta_c$, an incident electron from the $x < 0$ region can be reflected (transmitted) as a propagating state in $x < 0$ ($x > 0$) region. However, the number of transmitted propagating states varies from one to zero when $|\theta| > \theta_c$, indicating an abrupt change of scattering environment. As discussed in Ref. [41], this change generally results in a discontinuity in the derivative of the reflection amplitude. As a consequence, the Taylor expansion of the phase of the reflection amplitude around the critical incident angles $\pm\theta_c$ will be meaningless, making the anomalous spatial shifts obtained by linear approximation inaccurate.

To directly show this, we proceed to solve the scattering states of the graphene junction model Eq. (16), which can be written as [8]

$$\psi(\boldsymbol{k}) = \begin{cases} \psi^i(\boldsymbol{k}) + A_r\psi^r(\boldsymbol{k}), & x < 0 \\ A_t\psi^t(\boldsymbol{k}), & x > 0, \end{cases} \tag{18}$$

where $A_{r(t)}$ is the reflection (transmission) amplitude and ψ^i, ψ^r, and ψ^t are the basis states for incident, reflected, and transmitted states, respectively. Explicitly, the basis states read

$$\psi^i(\boldsymbol{k}) = \frac{1}{\sqrt{2}}\begin{pmatrix} e^{-i\theta/2} \\ e^{i\theta/2} \end{pmatrix} e^{ik_i x + ik_y y}, \tag{19}$$

$$\psi^r(\boldsymbol{k}) = \frac{1}{\sqrt{2}}\begin{pmatrix} -ie^{i\theta/2} \\ ie^{-i\theta/2} \end{pmatrix} e^{-ik_i x + ik_y y}, \tag{20}$$

$$\psi^t(\boldsymbol{k}) = \frac{1}{\sqrt{2}|E_F - V|}\begin{pmatrix} E_F - V \\ v(k_t + ik_y) \end{pmatrix} e^{ik_t x + ik_y y}. \tag{21}$$

Here $k_i = v^{-1}\sqrt{E_F - v^2k_y^2}$, $\theta = \arctan(k_y/k_i)$ is the incident angle, $k_t = v^{-1}\mathrm{sgn}(E_F - V)\sqrt{(E_F - V)^2 - v^2k_y^2}$ for $|\theta| < \theta_c$, and $k_t = i\kappa$ for $|\theta| > \theta_c$, where $\kappa = v^{-1}\sqrt{v^2k_y^2 - (E_F - V)^2}$. For the graphene junction model here, the boundary condition at the interface is

$$\psi(x = 0^-) = \psi(x = 0^+), \tag{22}$$

with which the reflection amplitude A_r is obtained as [8]

$$A_r = \frac{v(\kappa + k_y) + ie^{i\theta}(E_F - V)}{ve^{i\theta}(i\kappa + ik_y) + (E_F - V)}. \tag{23}$$

The square of the modulus of A_r ($|A_r|^2$) and the phase $\varphi = \arg(A_r)$ as functions of the incident angle are plotted in Figs. 2(c) and 2(d), respectively. One observes that for $|\theta| < \theta_c$, A_r is a finite real number with $\varphi = 0$, and for $|\theta| > \theta_c$, A_r becomes a complex number with $|A_r|^2 = 1$, indicating the appearance of total reflection. This is consistent with the fact that when $|\theta| > \theta_c$, there no longer exists a propagating mode for the transmitted state. Importantly, while both $|A_r|^2$ and φ are continuous functions, their derivatives are discontinuous at the critical angle $\pm\theta_c$ [see Figs. 2(c) and 2(d)], corresponding to an abrupt change of the scattering condition, namely, the disappearance of the transmitted propagating mode for $|\theta| > \theta_c$.

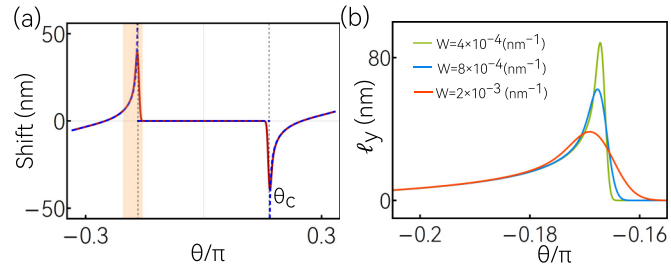

FIG. 3. The anomalous longitudinal shift in model Eq. (16). (a) The results obtained with linear approximation ℓ_y^{LA} (dashed line) and that obtained without approximation ℓ_y (solid line) versus incident angle. (b) ℓ_y versus θ for different beam width W. The box in (a) denotes the range of θ in (b). In the calculation, we choose $E_F = 100$ meV, $V = 150$ meV, $v = 10^6$ m/s.

Based on the expression of A_r, the longitudinal shift under linear approximation is obtained as [8]

$$\ell_y^{\mathrm{LA}} = 2\frac{\sin^2\theta + 1 - V/E_F}{\kappa\sin 2\theta}. \tag{24}$$

As discussed above, the accuracy of the anomalous shift obtained from linear approximation requires A_r to be an analytic function. But A_r is not an analytic function in the neighborhood of $\theta = \pm\theta_c$. Hence, Eq. (24) may be inaccurate around $\pm\theta_c$. In Fig. 3(a), we plot the typical behavior of the longitudinal shift ℓ_y^{LA} from Eq. (24), along with the shift ℓ_y obtained from Eq. (6) beyond linear approximation. We have checked that the wave packet of the reflected beam still features a Gaussian-type profile and is centered at same momentum with the incident wave packet. Hence, the shift obtained from Eq. (6) should be accurate. From Fig. 3(a), one observes that the ℓ_y^{LA} has two discontinuity points at $\pm\theta_c$. Specifically, it is zero for $|\theta| < \theta_c$, diverges abruptly at $\pm\theta_c$, and becomes finite when moving away from $\pm\theta_c$. In contrast, ℓ_y obtained from Eq. (6) is always continuous for any incident angle. Particularly, it is not divergent at $\pm\theta_c$, indicating the nonphysical divergent results from the linear approximation is resolved by using Eq. (6) to calculate the anomalous shift. Besides, there are several other observations. (i) At critical angle $\pm\theta_c$, while ℓ_y is not divergent, it still is very large and can reach a few tens of nanometers with reasonable parameters. (ii) Away from $\pm\theta_c$, ℓ_y^{LA} and ℓ_y share similar behavior and are almost identical, as shown in Fig. 3(a).

The anomalous shifts Eq. (24) obtained from linear approximation are always independent of the beam width ($\sim W = |\boldsymbol{W}|$). However, in optics, it has been demonstrated that the anomalous shifts around the critical parameters strongly depend on the beam width [42–44]. Here, we also calculate the longitudinal shift ℓ_y from Eq. (6) for different W. The obtained results are shown in Fig. 3(b), from which one can find that the maximum value of ℓ_y indeed varies with W_y, consistent with the results in optics. Again, when moving away from $\pm\theta_c$, ℓ_y is not sensitive to the value of W.

IV. TRANSVERSE SHIFT IN ANDREEV REFLECTION

In the second case, we consider the transverse shift in Andreev reflection [33,35]. In electronic systems, besides

ordinary electron scattering, Andreev reflection is another intriguing scattering process that occurs at the interface between metal and superconductor and is described by the Bogoliubov–de Gennes (BdG) equation. The junction model here is of a 3D electron gas interfaced with a d-wave superconductor. The corresponding BdG equation can be written as

$$H(x)\psi = \varepsilon\psi, \tag{25}$$

with ε the excitation energy

$$H = \begin{bmatrix} -\frac{1}{2m}\nabla^2 - E_F & 0 \\ 0 & -\mathcal{T}\big(-\frac{1}{2m}\nabla^2\big)\mathcal{T}^{-1} + E_F \end{bmatrix} \tag{26}$$

for normal metal region ($x < 0$), and

$$H = \begin{bmatrix} H_0 + V - E_F & \Delta(k_\parallel) \\ \Delta^*(k_\parallel) & -\mathcal{T}H_0\mathcal{T}^{-1} - V + E_F \end{bmatrix} \tag{27}$$

for the superconductor region ($x > 0$). In addition, the interface barrier potential $h\delta(x)$ is considered. Here, m denotes the electron mass, E_F is the Fermi energy, $\mathcal{T}$ is the time reversal operator, $H_0 = -\frac{1}{2m}(\partial_z^2 + \partial_y^2) - \frac{1}{2m_x}\partial_x^2$, $\Delta(k_y, k_z) = \Delta_0\cos(2\phi_k)$ represents a $d_{y^2-z^2}$ pairing with $\phi_k = \arctan(k_y/k_z)$, and V is a potential energy ensuring $E_F - V \gg \Delta_0$. According to the setup in Fig. 1, the rotation angle is identical to ϕ_k, namely, $\alpha = \phi_k$.

This model has been used to show that the transverse shift can be solely induced by the unconventional pairing, and it is found that by varying rotation angle α [see Fig. 1(b)], the transverse shift becomes divergent at certain critical angles. Here, we will show that the divergence is also caused by the change in the number of transmitted propagating states at the critical angles.

The scattering states of Eq. (25) can be written as [35]

$$\psi(\boldsymbol{k}) = \begin{cases} \psi^i(\boldsymbol{k}) + r_e\psi_e^r(\boldsymbol{k}) + r_h\psi_h^r(\boldsymbol{k}), & x < 0 \\ t_1\psi_1^t(\boldsymbol{k}) + t_2\psi_2^t(\boldsymbol{k}), & x > 0, \end{cases} \tag{28}$$

where $r_{e(h)}$ is the amplitude for the normal (Andreev) reflection, $t_{1(2)}$ is the transmission amplitude, and the ψ are the corresponding basis states, expressed as

$$\psi_e^r(\boldsymbol{k}) = \begin{pmatrix} 1 \\ 0 \end{pmatrix} e^{-ik_x^e x + ik_y y + ik_z z}, \tag{29}$$

$$\psi_h^r(\boldsymbol{k}) = \begin{pmatrix} 0 \\ 1 \end{pmatrix} e^{ik_x^h x + ik_y y + ik_z z}, \tag{30}$$

$$\psi_\pm^t(\boldsymbol{k}) = \begin{pmatrix} 1 \\ \eta_\pm \end{pmatrix} e^{ik_S^\pm x + ik_y y + ik_z z}, \tag{31}$$

where $\eta_\pm = \frac{\Delta_{\boldsymbol{k}_\pm}}{\varepsilon \pm \sqrt{\varepsilon^2 - \Delta_{k_S^\pm}^2}}$ with $\Delta_{\boldsymbol{k}_\pm} = \boldsymbol{\Delta}(k_\pm^S, k_y, k_z)$, $k_\parallel = \sqrt{k_y^2 + k_z^2}$, $k_x^{e/h} = \sqrt{2mE_F - k_\parallel^2}$, and $k_S^\pm = \pm\sqrt{2m_x(E_F - U - k_\parallel^2/2m)}$.

Before processing to the concrete calculations of the scattering amplitudes and the anomalous shifts, we discuss the influences of rotation angle and the value of excitation energy on the scattering in the interface. Since the d-wave superconductor is anisotropic in the $k_y - k_z$ plane, the band structure of the superconductor in different incident planes (determined by the rotation angle α) will be different, as shown in Figs. 4(a) and 4(b), indicating the transverse shift is sensitive to the rotation angles α and ϕ_k. We also plot the band gap $E_{\text{gap}} = |\Delta_{\boldsymbol{k}}|$ of the superconductor as a function of ϕ_k in Fig. 4(c), showing the superconductor becomes gapless at $\phi_k = \pm\pi/4,\ \pm 3\pi/4$. Then, a key observation is that for any excitation energy satisfying $|\varepsilon| < \Delta_0$, the two transmitted states (ψ_1^t and ψ_2^t) are propagating modes for $|\cos 2\phi| < \varepsilon/\Delta_0$ ($|\varepsilon| > E_{\text{gap}}$) and are evanescent modes for $|\cos 2\phi| > \varepsilon/\Delta_0$ ($|\varepsilon| < E_{\text{gap}}$), as illustrated in Fig. 4(c). In contrast, the two transmitted states are always propagating modes when $|\varepsilon| > \Delta_0$, as $|\varepsilon| > E_{\text{gap}}$ for any ϕ_k [see Fig. 4(d)]. Similarly, one can expect that the critical rotation angles for divergent transverse shifts in Ref. [35] satisfy $|\cos 2\phi_c| = \varepsilon/\Delta_0$ with $|\varepsilon| < \Delta_0$. Besides, when $|\varepsilon| > \Delta_0$, the transverse shifts obtained from linear approximation will be accurate and consistent with that obtained from Eq. (6).

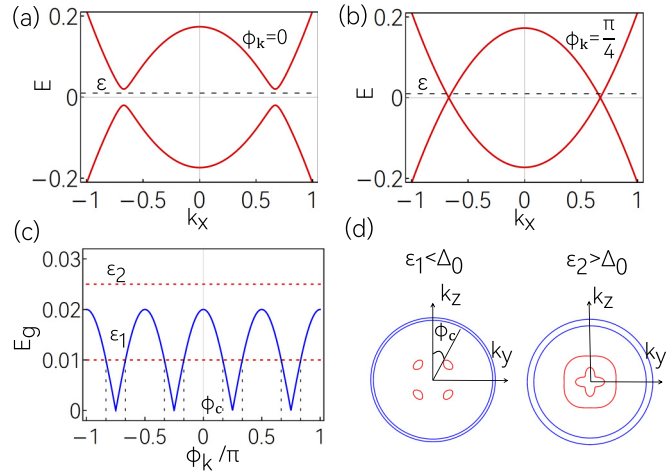

FIG. 4. Band structure of the BdG Hamiltonian in model Eq. (25). (a) and (b) show the BdG spectrum in different incident planes. (c) denotes the band gap E_g of the BdG spectrum. (d) The BdG Fermi surfaces with different excitation energies. In the calculation, we choose $\varepsilon = 10$ meV, $\Delta_0 = 20$ meV, $E_F = 0.4$ eV, $V = 0.2$ eV, $h = 0.3$ eV nm, and the incident angle $\theta = \pi/12$. We take the $\varepsilon_1 = 10$ meV, $\varepsilon_2 = 25$ meV in (c), (d).

With the boundary conditions,

$$\psi(x = 0^-) = \psi(x = 0^+), \tag{32}$$

$$\frac{1}{m}\partial_x\psi(x = 0^-) = \frac{1}{m_x}\partial_x\psi(x = 0^+) - h\psi(0), \tag{33}$$

the Andreev reflection amplitude r_h is obtained as [35]

$$r_h = \frac{-4\eta_-\eta_+\Gamma}{\eta_+(Z - 2\Gamma) - \eta_-(Z + 2\Gamma)}, \tag{34}$$

with $Z = 4\frac{mh}{k_e}^2 + 1 + \Gamma^2$ and $\Gamma = \frac{mk_s^+}{m_1 k_e}$.

In Fig. 5, we plot the obtained $|r_h|^2$ and $\varphi_h = \arg(r_h)$ as functions of the rotation angle ϕ_k for $|\varepsilon| < \Delta_0$ and $|\varepsilon| > \Delta_0$. We find that the derivative of $|r_h|^2$ and $\varphi_h = \arg(r_h)$ exhibit eight discontinuity points at $\phi_c = \pm[\arccos(\varepsilon/\Delta_0)]/2$ when $|\varepsilon| < \Delta_0$, but are smooth functions when $|\varepsilon| > \Delta_0$, consistent with the analysis of the band structure of the junction model. Interestingly, r_h is a pure real number when $|\varepsilon| > \Delta_0$. We

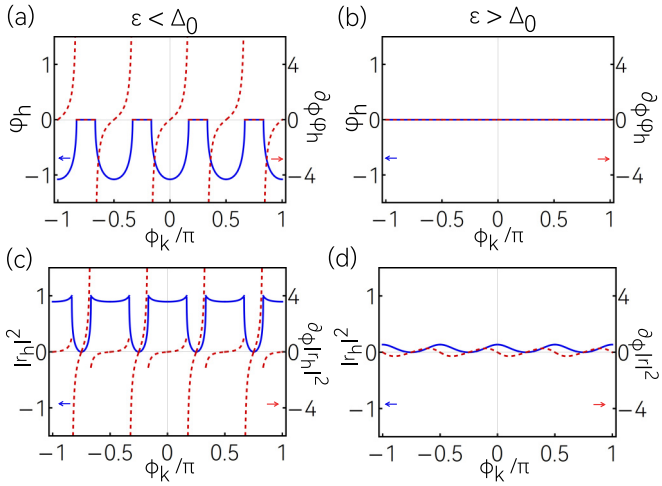

FIG. 5. (a), (b) The phase $\varphi_h = \arg(r_h)$ and its derivative and (c), (d) $|r_h|^2$ and its derivative versus ϕ_k in the cases of $|\varepsilon| < \Delta_0$ and $|\varepsilon| > \Delta_0$. Here, we choose $\Delta_0 = 20$ meV, $E_F = 0.4$ eV, $V = 0.2$ eV, $h = 0.3$ eV nm, and $\theta = \pi/12$. We take the $\varepsilon = 10$ meV in (a), (c) and $\varepsilon = 30$ meV in (b), (d).

then study the dependence of anomalous transverse shift on the rotation angle and ϕ_k.

Under the linear approximation, the anomalous transverse shift in Andreev reflection is established as [35]

$$\ell_T^{\mathrm{LA}} = -\frac{1}{k_\parallel}\partial_{\phi_k}\varphi_h = -\frac{\rho\Lambda\Delta_0^2\sin(4\phi_k)}{k_\parallel\varepsilon^2(1+\Lambda^2/\rho^2)}\Theta(|\Delta_0\cos 2\phi_k| - \varepsilon), \tag{35}$$

with $\rho = \varepsilon/\sqrt{\Delta_0^2\cos^2(2\phi_k) - \varepsilon^2}$ and $\Lambda = Z/(2\Gamma)$. According to Eq. (35), we find the transverse shift obtained from linear approximation ℓ_T^{LA} indeed is divergent at ϕ_c when $|\varepsilon| < \Delta_0$, as shown Fig. 6. For $\varepsilon > \Delta_0$, the transverse shift will be zero, as r_h is a real number with $\varphi_h = 0$.

The numerical results of the transverse shifts ℓ_T obtained from Eq. (6) with $|\varepsilon| < \Delta_0$ and different beam widths also are plotted in Fig. 6. We have checked that the wave packets of the reflected hole beam still can be well-defined and exhibit a Gaussian-type profile, indicating the calculated anomalous shift would be reliable. One observes that for all the beam

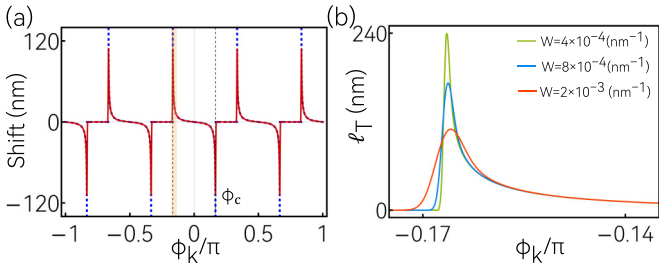

FIG. 6. The anomalous transverse shift in model Eq. (25). (a) The results obtained with linear approximation ℓ_T^{LA} (dashed line) and that obtained without approximation ℓ_T (solid line) versus ϕ_k. (b) ℓ_T versus ϕ_k for different beam widths W. The box in (a) denotes the range of ϕ_k in (b). Here, we choose $\varepsilon = 10$ meV, $\Delta_0 = 20$ meV, $E_F = 0.4$ eV, $V = 0.2$ eV, $h = 0.3$ eV nm, and $\theta = \pi/12$.

widths, the transverse shifts are not divergent at the critical angles ϕ_c. Similar to the first case, we find that (i) the anomalous shift indeed is significant at the critical angles and can reach a few tens of nanometers with reasonable parameters, (ii) ℓ_T and ℓ_T^{LA} are almost identical away from the critical angle ϕ_c, and (iii) the anomalous shift is sensitive to the beam width when and only when ϕ_k is close to α_c. Besides, when $|\varepsilon|/\Delta_0 > 1$, the transverse shifts ℓ_T obtained from Eq. (6) is negligible, consistent with the results from linear approximation.

V. ALTERNATIVE APPROXIMATION

In this section, we propose an alternative approximation to calculate the anomalous shifts, which is much less computationally expensive than the exact expression [Eq. (6)]. Meanwhile, the results obtained by the alternative approximation are always finite, solving the divergence problem of the linear approximation [Eq. (15)].

According to the above discussions, one knows that the dominating factor that affects the anomalous shifts is the phase rather than the absolute value of the scattering amplitudes. Hence, we may rewrite the reflected wave packet [Eq. (4)] as

$$\begin{aligned}\Psi^r(\boldsymbol{r},\boldsymbol{k}^c) &= \int w(\boldsymbol{k}-\boldsymbol{k}^c)A_r(\boldsymbol{k})\psi^r(\boldsymbol{k})d\boldsymbol{k}\\ &\approx |A_r(\boldsymbol{k}^c)|\int w(\boldsymbol{k}-\boldsymbol{k}^c)e^{i\varphi}\psi^r(\boldsymbol{k})d\boldsymbol{k}.\end{aligned} \tag{36}$$

Based on this approximate reflected wave packet, the expression of the anomalous shifts can be established as

$$\boldsymbol{\ell}^{\mathrm{alter}} = \frac{1}{\mathcal{N}}\int d\boldsymbol{k}w^2(\boldsymbol{k}-\boldsymbol{k}^c)\times\boldsymbol{\Pi}(\boldsymbol{k}), \tag{37}$$

where $\mathcal{N} = \int d\boldsymbol{k}w^2(\boldsymbol{k}-\boldsymbol{k}^c)$, and $\boldsymbol{\Pi}(\boldsymbol{k})$ is the shift vector [40],

$$\boldsymbol{\Pi}(\boldsymbol{k}) = \boldsymbol{A}_r - \boldsymbol{A}_i - \frac{\partial\varphi}{\partial\boldsymbol{k}} = \sum_n\left[v_n^i\partial_{\boldsymbol{k}}\phi_n^i - v_n^r\partial_{\boldsymbol{k}}\left(\phi_n^r+\varphi\right)\right], \tag{38}$$

with $\boldsymbol{A}_{i(r)} = i\langle u^{i(r)}|\partial_{\boldsymbol{k}}|u^{i(r)}\rangle$ the Berry connection. In the derivation, we have used the following formula [45]:

$$\langle\psi(\boldsymbol{k}')|\boldsymbol{r}|\psi(\boldsymbol{k})\rangle = \delta(\boldsymbol{k}-\boldsymbol{k}')\boldsymbol{A}(\boldsymbol{k}) + i\frac{\partial}{\partial\boldsymbol{k}}\delta(\boldsymbol{k}-\boldsymbol{k}'). \tag{39}$$

Notice that if the shift vector $\boldsymbol{\Pi}(\boldsymbol{k})$ is a smooth function of the momentum $\boldsymbol{k}$, the anomalous shifts from linear approximation and the approximation provided here would be identical, i.e., $\boldsymbol{\ell}^{\mathrm{alter}} = \boldsymbol{\ell}^{\mathrm{LA}} = \boldsymbol{\Pi}(\boldsymbol{k}_c)$. In contrast, when $\boldsymbol{\Pi}(\boldsymbol{k})$ is divergent at certain momentum $\boldsymbol{K}$, there will exit significant deviation between $\boldsymbol{\ell}^{\mathrm{alter}}$ and $\boldsymbol{\ell}^{\mathrm{LA}}$ in the vicinity of $\boldsymbol{K}$.

Since the calculations of $\boldsymbol{\ell}^{\mathrm{alter}}$ do not require the spatial distribution of the incident and reflected wave packets, it is more convenient than the exact expression [Eq. (6)]. Furthermore, because the divergence of anomalous shifts generally takes the form of $\sim 1/k$, $\boldsymbol{\ell}^{\mathrm{alter}}$ will be always finite due to the integral on $\boldsymbol{k}$. In Fig. 7, we plot the anomalous shifts calculated from the three different methods. One can find that far away from the critical (divergent) point, the results obtained by the three methods have negligible differences. Around the critical

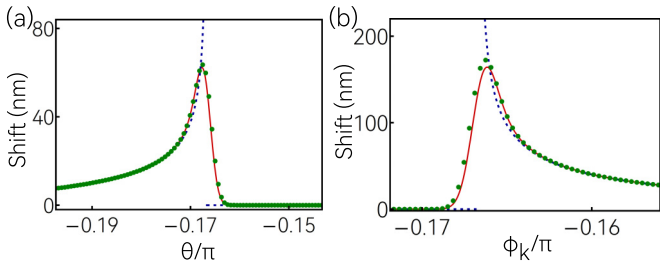

FIG. 7. The anomalous shift in (a) model Eq. (16) and (b) model Eq. (25), which are obtained from three different methods. The blue dashed curves are the results from linear approximation. Green dotted and red solid curves denote the shifts calculated by Eqs. (6) and (37), respectively. Here, the beam width $W = 8 \times 10^{-4}$ nm^{-1}, and the other parameters in (a) and (b) are the same as those in Figs. 3 and 6, respectively.

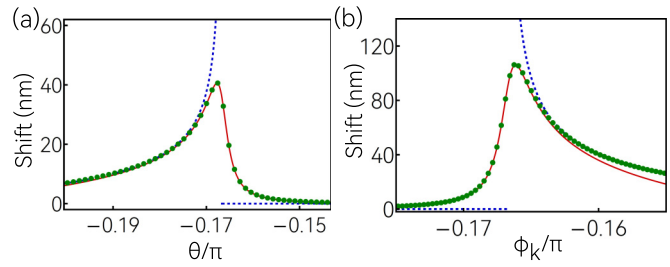

FIG. 8. The anomalous shift in (a) model Eq. (16) and (b) model Eq. (25), which are calculated from Cauchy-form wave packet. The blue dashed curves are the results from linear approximation. Red solid curves show the analysis results of (a) Eq. (42) and (b) Eq. (44). Green dotted curves denote the shifts calculated from Eq. (37). Here, the beam width $W = 8 \times 10^{-4}$ nm^{-1}, and the other parameters in (a) and (b) are the same as those in Figs. 3 and 6, respectively.

point, the shift from linear approximation diverges. However, the shifts from both Eqs. (6) and (37) are finite, and are almost identical for all the momenta (angles).

More importantly, with a suitable wave-packet profile, such as Cauchy form, we can analytically obtain the results of $\boldsymbol{\ell}^{\text{alter}}$. The wave-packet profile with Cauchy form reads

$$w(\boldsymbol{k}) = \prod_{i=y,z} \left(\frac{1}{\pi} \frac{W_i}{k_i^2 + W_i^2} \right)^{1/2}, \tag{40}$$

with W_i the Cauchy width. According to the Laurent series expansion, the shift vector around the critical angle (θ_c) reads

$$\Pi_y \approx a_0(k_c)(k_c - k_y)^{-\frac{1}{2}} - a_1(k_c)(k_c - k_y)^{\frac{1}{2}}, \tag{41}$$

for the model Eq. (16) with $a_0 = \frac{\xi}{\sqrt{|2k_y|}}$, $a_1 = \frac{-\xi + 4k_y \partial_{k_y} \xi}{4k_y \sqrt{|2k_y|}}$, $\xi = 2\frac{1+\sin^2\theta - V/E_F}{\sin 2\theta}$, $k_y = E_F \sin\theta/v$, and $k_c = E_F \sin\theta_c/v$. Then the longitudinal shift can be analytically obtained:

$$\begin{aligned} \boldsymbol{\ell}_y^{\text{alter}} &= \frac{1}{\mathcal{N}} \int_{-\infty}^{\infty} dk_y \frac{1}{\pi} \frac{W_y}{(k_c - k_y)^2 + W_y^2} \Pi_y \\ &= -a_0(k_c) \text{Im}\left[\frac{1}{\sqrt{iW_y - (k_c - k_y)}} \right] \\ &\quad -a_1(k_c) \text{Im}[\sqrt{iW_y - (k_c - k_y)}]. \end{aligned} \tag{42}$$

Similarly, the transverse shift of the model Eq. (25) around the critical angle (ϕ_c) reads

$$\Pi_\phi \approx b_0(\phi_c)(\phi_k - \phi_c)^{-\frac{1}{2}} - b_1(\phi_c)(\phi_k - \phi_c)^{\frac{1}{2}}, \tag{43}$$

with $b_0 = \frac{\zeta}{\sqrt{|2\sin 4\phi_k|}}$, $b_1 = \frac{\cot 4\phi_k \zeta - \partial_{\phi_k}\zeta}{\sqrt{|2\sin 4\phi_k|}}$, and $\zeta = -\frac{\Lambda\Delta_0 \sin 4\phi_k}{k_\parallel \varepsilon(1+\Lambda^2\rho^{-2})}$. Note that to guarantee the transverse shift is finite, the condition $|\cos 2\phi_k| > \varepsilon/\Delta_0$ is imposed. Then the transverse shift can be established as

$$\begin{aligned} \boldsymbol{\ell}_\phi^{\text{alter}} &= \frac{1}{\mathcal{N}} \int_{-\infty}^{\infty} d\phi_k \frac{1}{\pi} \frac{W_\phi}{(\phi_c - \phi_k)^2 + W_\phi^2} \Pi_\phi \\ &= -b_0(\phi_c) \text{Im}\left[\frac{1}{\sqrt{iW_\phi - (\phi_k - \phi_c)}} \right] \\ &\quad -b_1(\phi_c) \text{Im}[\sqrt{iW_\phi - (\phi_k - \phi_c)}]. \end{aligned} \tag{44}$$

In the derivation, we have used the approximation $\int_{-|\eta|}^{|\eta|} w(x)f(x)dx \approx \int_{-\infty}^{\infty} w(x)f(x)dx$ with η a finite value and $w(x)$ denoting the Cauchy distribution.

Remarkably, from the analytical expressions, we find that around the critical angles, there is a simple power law between the anomalous shift and beam width:

$$\ell \propto W^{-\frac{1}{2}}. \tag{45}$$

The results of the analytical expressions are plotted in Fig. 8, along with the results from linear approximation and that numerically obtained from Eq. (37). One observes that the analytical results match well with the numerical results around the critical angles, where the shift vector is expanded. We also present a log-log plot of the anomalous shift versus beam width in Fig. 9, which clearly demonstrates the $-1/2$ power law between the anomalous shift and the beam width.

VI. CONCLUSIONS

In this paper, we study the anomalous shift in interface electronic reflection based on the quantum scattered

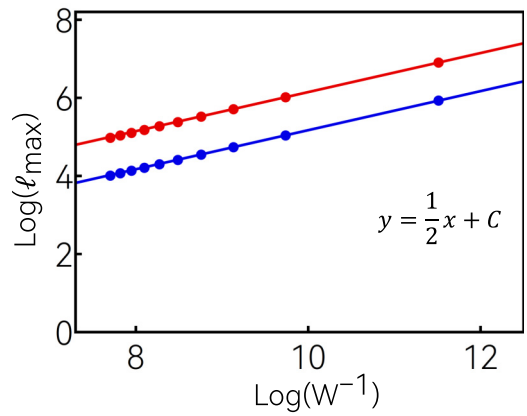

FIG. 9. Log-Log plot of the maximum value of the anomalous shift ℓ versus beam width W, which are calculated from Cauchy-form wave packet. Red and blue curves denote the analytical expressions of Eqs. (42) and (44), while the gray dots represent the results obtained from Eq. (37).

approach with and without linear approximation. We find that for a large case of junction models, the propagating modes of scattering states may be changed by varying certain parameters like the incident angle. Around the critical parameters, the linear approximation is invalid and leads to divergent anomalous shifts in scattering. In contrast, the quantum scattered approach without linear approximation always gives more accurate results, which are significant but not divergent around the critical parameters. Moreover, we show the anomalous shifts around the critical parameters decrease when increasing the width of the incident beam. This means that the narrower the incident beam, the more pronounced the anomalous shift. Away from the critical parameters, the anomalous shifts obtained from the quantum scattered approach with and without linear approximation are similar and not sensitive to the beam width.

ACKNOWLEDGMENTS

The authors thank J. Xun for helpful discussions. This work was supported by the NSF of China (Grant No. 12004035), and the National Natural Science Fund for Excellent Young Scientists Fund Program (Overseas).

[1] K. Y. Bliokh and A. Aiello, J. Opt. **15**, 014001 (2013).
[2] F. Goos and H. Hänchen, Annalen der Physik **436**, 333 (1947).
[3] R. H. Renard, J. Opt. Soc. Am. **54**, 1190 (1964).
[4] F. Fedorov, Dokl. Akad. Nauk SSSR **105**, 465 (1955).
[5] C. Imbert, Phys. Rev. D **5**, 787 (1972).
[6] S. Onoda, S. Murakami, and N. Nagaosa, Phys. Rev. Lett. **93**, 167602 (2004).
[7] S. C. Miller and N. Ashby, Phys. Rev. Lett. **29**, 740 (1972).
[8] C. W. J. Beenakker, R. A. Sepkhanov, A. R. Akhmerov, and J. Tworzydło, Phys. Rev. Lett. **102**, 146804 (2009).
[9] X. Chen, X.-J. Lu, Y. Ban, and C.-F. Li, J. Opt. **15**, 033001 (2013).
[10] Z. Wu, F. Zhai, F. M. Peeters, H. Q. Xu, and K. Chang, Phys. Rev. Lett. **106**, 176802 (2011).
[11] Z.-M. Yu, Y. Liu, and S. A. Yang, Front. Phys. **14**, 33402 (2019).
[12] U. Chattopadhyay, L.-k. Shi, B. Zhang, J. C. W. Song, and Y. D. Chong, Phys. Rev. Lett. **122**, 066602 (2019).
[13] N. K. Dongre and K. Roychowdhury, Phys. Rev. B **106**, 075414 (2022).
[14] J. Huang, Z. Duan, H. Y. Ling, and W. Zhang, Phys. Rev. A **77**, 063608 (2008).
[15] Victor-O. de Haan, J. Plomp, T. M. Rekveldt, W. H. Kraan, A. A. van Well, R. M. Dalgliesh, and S. Langridge, Phys. Rev. Lett. **104**, 010401 (2010).
[16] C.-K. Chiu, J. C. Y. Teo, A. P. Schnyder, and S. Ryu, Rev. Mod. Phys. **88**, 035005 (2016).
[17] N. P. Armitage, E. J. Mele, and A. Vishwanath, Rev. Mod. Phys. **90**, 015001 (2018).
[18] X. Wan, A. M. Turner, A. Vishwanath, and S. Y. Savrasov, Phys. Rev. B **83**, 205101 (2011).
[19] Z.-M. Yu, Y. Yao, and S. A. Yang, Phys. Rev. Lett. **117**, 077202 (2016).
[20] H. Weng, Y. Liang, Q. Xu, R. Yu, Z. Fang, X. Dai, and Y. Kawazoe, Phys. Rev. B **92**, 045108 (2015).
[21] W. Wu, Y. Liu, S. Li, C. Zhong, Z.-M. Yu, X.-L. Sheng, Y. X. Zhao, and S. A. Yang, Phys. Rev. B **97**, 115125 (2018).
[22] A. A. Soluyanov, D. Gresch, Z. Wang, Q. Wu, M. Troyer, X. Dai, and B. A. Bernevig, Nature (London) **527**, 495 (2015).
[23] X.-P. Li, K. Deng, B. Fu, Y. K. Li, D.-S. Ma, J. Han, J. Zhou, S. Zhou, and Y. Yao, Phys. Rev. B **103**, L081402 (2021).
[24] X.-P. Li, B. Fu, D.-S. Ma, C. Cui, Z.-M. Yu, and Y. Yao, Phys. Rev. B **103**, L161109 (2021).
[25] Z.-M. Yu, Z. Zhang, G.-B. Liu, W. Wu, X.-P. Li, R.-W. Zhang, S. A. Yang, and Y. Yao, Sci. Bull. **67**, 375 (2022).
[26] G.-B. Liu, Z. Zhang, Z.-M. Yu, S. A. Yang, and Y. Yao, Phys. Rev. B **105**, 085117 (2022).
[27] Z. Zhang, G.-B. Liu, Z.-M. Yu, S. A. Yang, and Y. Yao, Phys. Rev. B **105**, 104426 (2022).
[28] Q.-D. Jiang, H. Jiang, H. Liu, Q.-F. Sun, and X. C. Xie, Phys. Rev. Lett. **115**, 156602 (2015).
[29] S. A. Yang, H. Pan, and F. Zhang, Phys. Rev. Lett. **115**, 156603 (2015).
[30] Y.-R. Hao, L. Wang, and D.-X. Yao, Phys. Rev. B **99**, 165406 (2019).
[31] X. Feng, Y. Liu, Z.-M. Yu, Z. Ma, L. K. Ang, Y. S. Ang, and S. A. Yang, Phys. Rev. B **101**, 235417 (2020).
[32] Y. Liu, Z.-M. Yu, C. Xiao, and S. A. Yang, Phys. Rev. Lett. **125**, 076801 (2020).
[33] Y. Liu, Z.-M. Yu, and S. A. Yang, Phys. Rev. B **96**, 121101 (2017).
[34] Y. Liu, Z.-M. Yu, H. Jiang, and S. A. Yang, Phys. Rev. B **98**, 075151 (2018).
[35] Z.-M. Yu, Y. Liu, Y. Yao, and S. A. Yang, Phys. Rev. Lett. **121**, 176602 (2018).
[36] Y. Liu, Z.-M. Yu, J. Liu, H. Jiang, and S. A. Yang, Phys. Rev. B **98**, 195141 (2018).
[37] X. Liu, S. Dutta Gupta, and G. S. Agarwal, Phys. Rev. A **89**, 013824 (2014).
[38] H. Luo, X. Zhou, W. Shu, S. Wen, and D. Fan, Phys. Rev. A **84**, 043806 (2011).
[39] X. Ling, W. Xiao, S. Chen, X. Zhou, H. Luo, and L. Zhou, Phys. Rev. A **103**, 033515 (2021).
[40] L.-k. Shi and J. C. W. Song, Phys. Rev. B **100**, 201405(R) (2019).
[41] Z.-M. Yu, D.-S. Ma, H. Pan, and Y. Yao, Phys. Rev. B **96**, 125152 (2017).
[42] H. M. Lai, F. C. Cheng, and W. K. Tang, J. Opt. Soc. Am. A **3**, 550 (1986).
[43] L.-G. Wang, S.-Y. Zhu, and M. S. Zubairy, Phys. Rev. Lett. **111**, 223901 (2013).
[44] X. Qiu, L. Xie, J. Qiu, Z. Zhang, J. Du, and F. Gao, Opt. Express **23**, 18823 (2015).
[45] J. E. Sipe and A. I. Shkrebtii, Phys. Rev. B **61**, 5337 (2000).